TOXICOLOGICAL SCIENCES, 164(1), 2018, 339–352

doi: 10.1093/toxsci/kfy090
Advance Access Publication Date: April 14, 2018
Research Article

Hydroxylated-Graphene Quantum Dots Induce DNA Damage and Disrupt Microtubule Structure in Human Esophageal Epithelial Cells

Ming Li,[*,†,1] Meng-Meng Gu,[*,†,1] Xin Tian,[*,†,1] Bei-Bei Xiao,[*,†] Siyuan Lu,[*,†] Wei Zhu,[*,†] Lan Yu,[‡,2] and Zeng-Fu Shang[*,†,2]

[*]State Key Laboratory of Radiation Medicine and Protection, Department of Radiobiology, School of Radiation Medicine and Protection, Medical College of Soochow University, Suzhou 215123, People's Republic of China; [†]Collaborative Innovation Center of Radiation Medicine of Jiangsu Higher Education Institutions, Soochow University, Suzhou 215123, People's Republic of China; and [‡]Suzhou Digestive Diseases and Nutrition Research Center, Nanjing Medical University Affiliated Suzhou Hospital, North District of Suzhou Municipal Hospital, Suzhou 215000, People's Republic of China

[1]These authors contributed equally to this study.
[2]To whom correspondence should be addressed at Suzhou Digestive Diseases and Nutrition Research Center, Nanjing Medical University Affiliated Suzhou Hospital, North District of Suzhou Municipal Hospital, No. 242 Guangji Road, Suzhou 215000, People's Republic of China. Fax: +86-512-65332028; E-mail: Yulan_229@163.com and State Key Laboratory of Radiation Medicine and Protection, Department of Radiobiology, School of Radiation Medicine and Protection, Medical College of Soochow University, No. 199 Ren'ai Road, Suzhou 215123, People's Republic of China. Fax: +86 512 658 84830. E-mail: zengfu.shang@suda.edu.cn.

ABSTRACT

Graphene quantum dots (GQDs) have attracted significant interests due to their unique chemical and physical properties. In this study, we investigated the potential effects of hydroxyl-modified GQDs (OH-GQDs) on the human esophageal epithelial cell line HET-1A. Our data revealed significant cytotoxicity of OH-GQDs which decreased the viability of HET-1A in a dose and time-dependent manner. The moderate concentration (25 or 50 μg/ml) of OH-GQDs significantly blocked HET-1A cells in G_0/G_1 cell cycle phase. An increased percentage of γH2AX-positive and genomically unstable cells were also detected in cells treated with different doses of OH-GQDs (25, 50, and 100 μg/ml). Microarray data revealed that OH-GQDs treatment down-regulated genes related to DNA damage repair, cell cycle regulation and cytoskeleton signal pathways indicating a novel role of OH-GQDs. Consistent with the microarray data, OH-GQDs disrupted microtubule structure and inhibited microtubule regrowth around centrosomes in HET-1A cells. In conclusion, our findings provide important evidence for considering the application of OH-GQDs in biomedical fields.

Key words: OH-GQDs; DNA damage; cell cycle regulation; microtubule structure; esophageal epithelial cells.

As a new member of the graphene family, graphene quantum dots (GQDs) have emerged as an attractive material in many biomedical fields due to their unique physicochemical properties and good biocompatibility (Li *et al.*, 2011; Madani *et al.*, 2013; Markovic *et al.*, 2012; Shen *et al.*, 2012; Zheng *et al.*, 2013). For instance, many studies have reported the efficacy of GQDs in drug delivery. One study showed that GQDs-doxorubicin (Dox) conjugates enhanced the nuclear uptake and DNA cleavage efficiency of Dox (Wang *et al.*, 2013) and another by Wang *et al.* (2013) proved that PEGylated GQDs had higher loading capacity and released Dox in a pH-responsive manner. Modifying GQDs with specific ligands can increase tumor cells targeted drug delivery. Wang *et al.* (2014) functionalized GQDs with folic acid (FA) and their *in vitro* data showed that Dox-GQD-FA nano-complex could be specifically targeted to the tumor cells thus decreasing the cytotoxicity in nontarget cells. Abdullah-Al-Nahain *et al.* (2013) developed a new targeting strategy by modifying GQDs with hyaluronic acid (HA) which can bind to the CD44 antigen, a recognized cancer stem cells marker highly correlated with chemo-resistance (Vinogradov and Wei, 2012). They were able to show enhanced fluorescence of the HA-GQDs in a tumor-environment compared with GQDs alone in an *in vivo* system (Abdullah-Al-Nahain *et al.*, 2013). In addition to their role in drug delivery, GQDs can also be used as a therapeutic agent via production of $^1O_2$ in a multistate sensitization process (Ge *et al.*, 2014). Moreover, the study of Zhou et al (Zhou *et al.*, 2012) suggested that GQDs have better DNA cleavage activity than graphene oxide (GO), which has added to our knowledge of the interaction between GQDs and biological systems.

One of the major concerns regarding the biological applications of GQDs is their potential toxicity. Recent studies have focused on the toxicological properties of both raw and surface doped GQDs nanomaterials (Chong *et al.*, 2014; Jiang *et al.*, 2015; Kim *et al.*, 2016; Qin *et al.*, 2015; Qiu *et al.*, 2016; Tian *et al.*, 2016; Wang *et al.*, 2015, 2016; Wu *et al.*, 2013; Yuan *et al.*, 2014; Zhao *et al.*, 2015; Zhu *et al.*, 2011). Although many of these studies indicate good biocompatibility of the GQDs, we and several other groups demonstrated that raw and modified GQDs exhibit obvious cytotoxicity in certain biosystems. For instance, Wang *et al.* (2015) showed that GQDs can induce the generation of reactive oxygen species (ROS) and stimulate the expression of several DNA damage response proteins (p53, Rad51, and OGG1) in NIH3T3 cells. Using macrophages as a model, it has also been shown that GQDs promote intracellular ROS generation and activate apoptosis and autophagy signal pathways (Qin *et al.*, 2015). Our recent study demonstrated that hydroxyl-modified GQDs (OH-GQDs) can significantly inhibit the viability of A549 and H1299 cells (Tian *et al.*, 2016). OH-GQDs promote nuclear accumulation of the p53 protein (Tian *et al.*, 2016), an important tumor suppressor that maintains genetic stability after DNA damage, indicating the activation of p53-dependent transcription. All these data indicate that GQDs might be potentially genotoxic, although the precise genotoxic effects of GQDs and its underlying molecular mechanism are still not fully known.

In this study, we evaluated the genotoxicity of OH-GQDs on cells due to its potential medical application, such as drug delivery. Oral administration is a preferred mode of drug delivery in humans. Esophageal is one of the important organs to expose to the drugs. We found that OH-GQDs significantly inhibited the viability of human esophageal epithelial HET-1A cells. OH-GQDs blocked cell cycle progression at G_0/G_1 phase and induced a dose-dependent increase in DNA damage signals. A 24 h treatment with OH-GQDs (100 μg/ml) caused a dramatic increase in micronucleated cells. To further clarify the potential biological mechanism of OH-GQDs' genotoxicity, mRNA microarray was performed on control and OH-GQDs-treated HET-1A cells which revealed that OH-GQDs treatment altered the gene expression profile related to DNA damage repair and cell cycle regulation pathways. More interestingly, we discovered that cytoskeleton-related genes were downregulated by OH-GQDs. Consistent with these results, OH-GQDs disrupted microtubule structure and inhibited microtubule regrowth in HET-1A cells. Taken together, our data provide novel insights into how GQDs communicate with the biological system.

MATERIALS AND METHODS

Characterization of the OH-GQDs. The OH-GQDs were purchased from XFNANO Materials Tech Co. (Nanjing, China) and their physical properties were characterized by transmission electron microscopy (TEM; Tecnai G-20; FEI, Hillsboro, Oregon) and atomic force microscopy (AFM; Nanoscope Icon; Veeco, Plainview, New York). The hydrodynamic size of OH-GQDs was determined by a dynamic light scatting (DLS) instrument. Prior to use, the OH-GQDs were ultra-sonicated for 5 min and vortexed for 1 min.

Cell culture and treatment. The human esophageal squamous epithelial cell line HET-1A was kindly provided by Dr Jundong Zhou of the Nanjing Medical University Affiliated Suzhou Hospital Cancer Medical Central Laboratory (Suzhou, China). LO2, HIEC-6 and ECA-109 cells were preserved in our laboratory. The cells were maintained in RPMI 1640 or DMEM medium (Hyclone, Hudson, New Hamphire) supplemented with 10% fetal bovine serum (Gibco, Rockville, Maryland) in a humidified atmosphere at 37 °C and 5% CO_2. The cells were treated with varying concentrations of OH-GQDs for different durations.

Cellular uptake assays. To determine the cellular uptake of OH-GQDs, HET-1A cells were plated on a confocal dish and cultured overnight. Next, OH-GQDs were added to the dish for incubation in culture medium for 24 h. Then the cells were observed by a fluorescence microscope (IX73; Olympus, Tokyo, Japan).

The internalized OH-GQDs were also estimated by comparing the side scattered light (SSC) signals between OH-GQDs-treated and -untreated cells through flow cytometry. The procedures are as follow: the cells were washed 3 times with PBS 24 h post OH-GQDs exposure. Cells were harvested and fixed with 4% formaline solution and then resuspended in PBS buffer for flow cytometry measurements (BD Biosciences, San Diego, CA, USA).

Cell viability measurement. Cell Counting Kit-8 (CCK-8; Dojindo Laboratories, Kyushu, Japan) was used to assess the cell viability according to the manufacturer's instructions. Briefly, cells were seeded in a 96-well plate at a density of 3×10^3 cells per well and incubated overnight. The OH-GQDs were added at the indicated concentrations (0, 25, 50, 100, and 200 μg/ml) and the cells were further incubated for 24 h or 48 h. After the stipulated time, 10 μl of CCK-8 solution was added to each well and incubated for 2 h. The absorbance values (OD450) were measured using a VersaMax Microplate Reader (BioTek, Winooski, Vermont).

Cell cycle distribution analysis. HET-1A cells were seeded in a 6-well plate at a density of 1.0×10^5 cells per well in triplicates and cultured overnight. After being treated with 25 and 50 μg/ml OH-GQDs for 24 and 48 h, cells were collected and fixed in 70% ethanol overnight at −20 °C. The control cells were plated and harvested at the same time as OH-GQDs-treated cells. The fixed cells were washed and resuspended in PBS containing RNase A (100 μg/ml) and propidium iodide (PI, 50 μg/ml) (Sigma-Aldrich, St Louis, Missourio). After incubation for 30 min in the dark, cells were analyzed by FACSVerse Flow Cytometer (BD Biosciences, San Diego, California).

Apoptosis detection. HET-1A cells were seeded in 6-well plates and treated with different doses of OH-GQDs (0, 25, 50, and 100 μg/ml) for 24 h. Then the FITC Annexin V Apoptosis Detection Kit (BD, Pharmingen, San Diego, California) was used for the detection of apoptosis according to the manufacturer's protocol.

The cells were harvested and resuspended in 100 μl 1 × binding buffer. Then 5 μl of FITC-conjugated Annexin V and 5 μl of PI were added. Cells were incubated in the dark for 15 min at room temperature. After addition of 400 μl of 1 × binding buffer, cells were analyzed by flow cytometry (FACSVerse; BD Biosciences).

Measurement of intracellular ROS generation. HET-1A cells were seeded into 3.5-cm dishes and treated with 25 and 50 μg/ml OH-GQDs for 24 and 48 h. Then cells were incubated with 200 μl of 100 μM DCFH-DA (Sigma-Aldrich) at 37 °C for 30 min. The control cells were plated and harvested at the same time as OH-GQDs-treated cells. After the aspiration of the DCFH-DA, cells were harvested and the ROS probe was detected by flow cytometry (FACSVerse; BD Biosciences). The data were presented as the average ROS intensity.

Immunofluorescent staining. HET-1A cells were seeded in a 6-well plate containing poly-D-Lysine-coated cover slides and treated with different concentrations of OH-GQDs (0, 25, 50, and 100 μg/ml) for 24 h. The slides were washed twice in PBS and fixed in 4% paraformaldehyde/PBS at room temperature for 30 min. After permeabilization with 0.5% Triton X-100/PBS at room temperature for 15 min, the cells were blocked with 5% bovine serum albumin/PBS at room temperature for 1 h. The slides were incubated with anti α-tubulin, γ-tubulin (Sigma-Aldrich) or γH2AX (Abcam, Cambridge, Massachusetts) antibodies (1:1000) for 4 h at room temperature. After being washed 3 times with PBS, the cells were then incubated with Alexa-488 conjugated anti-rabbit or Alexa-568 conjugated anti-mouse secondary antibodies (Invitrogen, Carlsbad, California) for 1 h at room temperature. The slides were counterstained with DAPI (Vector Laboratories, Burlingame, California) for visualization of DNA and imaged under a FV1200 laser-scanning confocal microscope (Olympus, Tokyo, Japan).

The cytokinesis-blocked micronucleus assay. After being treated with different concentrations of OH-GQDs (0, 25, 50, and 100 μg/ml) for 24 h, the HET-1A cells were harvested and suspended with 10 ml of 75 mM KCl for 5 min at room temperature. The cells were fixed in 5 ml of Carnoy's solution (1:3 mixtures of ice-cold acetic acid and methanol) for 40 min, then dropped onto slides, air-dried and stained with Giemsa. A total of 200 mitotic cells per sample were examined under ordinary optical microscope, and the micronucleus frequency was reported as the percentage of micronucleated cells in mitotic cells.

Protein extraction and Western blot. Protein extraction and Western blot were performed as previously described in Li *et al.* (2015). The following primary antibodies were used: Cyclin A2, Cyclin B1, Cyclin D2, FANCD2, ataxia telangiectasia-mutated (ATM) (Cell Signaling Technology, Beverly, Massachusetts), DNA-dependent protein kinase catalytic subunit (DNA-PKcs) (Santa Cruz Biotechnology, Santa Cruz, California), γ-H2AX (Abcam), H2AX (Novus Biologicals, Littleton, Colorado) and GAPDH (Beyotime Institute of Biotechnology, Haimen, China). All primary antibodies except DNA-PKcs were used at a dilution of 1000-fold. The DNA-PKcs antibody was used at a 500-fold dilution.

Microtubule regrowth assay. Microtubule regrowth assays were performed as previously described in Shang *et al.* (2014). HET-1A cells were plated onto coated cover slides in 3.5-cm dishes and incubated with ice-cold medium supplemented with 1 μg/ml nocodazole (Sigma-Aldrich) for 1 h. Prewarmed fresh medium containing 25 and 50 μg/ml OH-GQDs was added after washing with PBS. At indicated times (0, 4, and 8 min) after treatment with OH-GQDs, cells were fixed in ice-cold methanol and subjected to immunofluorescent staining as described earlier.

Table 1. Primer Sequences for qRT-PCR Analysis

Gene Name	Primer Sequences
GAPDH	F: 5′-CAACTACATGGTCTACATGTTCC-3′ R: 5′-CAACCTGGTCCTCAGTGTAG-3′
SLC6A13	F: 5′-TGGGGAGATCATTGGCTTAG-3′ R: 5′-AGAGGAAGACGAGGTAGGGG-3′
USP31	F: 5′-CTGGAGTACACCCCGCAG-3′ R: 5′-CAGAAACTCCTGGGCATCAT-3′
GADD45B	F: 5′-ACAGTGGGGGTGTACGAGTC-3′ R: 5′-GATGTCATCCTCCTCCTCCTC-3′
ATF3	F: 5′-GGCCAGACAAACAGCCC-3′ R: 5′-ACTTCCGAGGCAGAGACCTG-3′
SH3MD1	F: 5′-AGGAACCCCTCCAAGCACTA-3′ R: 5′-CTGCATCTGCAGGTCAAAGA-3′
FANCF	F: 5′-GCTAGTCCACTGGCTTCTGG-3′ R: 5′-GGTGGCGGCTAGTCACTAAA-3′

Microarray. HET-1A cells were seeded in 6-cm dishes and treated with 50 μg/ml OH-GQDs or equivalent volume of vehicle in triplicates and harvested after 24 h. Total RNA was extracted for gene expression profiling using the Agilent SurePrint G3 Human Gene Expression v3 (8*60K; Agilent Technologies, Santa Clara, California). Total RNA labeling and array hybridization were performed using standard protocols according to the manufacturers' instructions. The Agilent Scanner G2505C was used to scan the probe arrays and Agilent Feature Extraction software (version 10.7.1.1) was used to analyze array images to get raw data. Quantile normalization and subsequent data processing were performed using the GeneSpring software package (version 13.1, Agilent Technologies). After quantile normalization of the raw data, the probes that at least 100% of the values in any 1 out of all conditions have flags in "Detected" were chosen for further data analysis. Differentially expressed genes were then identified through fold change and p values were calculated using t test. The threshold set for up- and down-regulated genes was a fold change ≥ 2.0 and a p value $\leq .05$. Afterwards, gene ontology (GO) analysis and Kyoto Encyclopedia of Genes and Genomes pathway analysis were applied to determine the roles of these differentially expressed mRNAs. Finally, Hierarchical Clustering was performed to display the distinguishable genes' expression pattern across samples. Microarray data were available on the GEO database: accession number GSE96720.

RNA isolation and quantitative real-time polymerase chain reaction assay. Total RNA was extracted by mirVana RNA Isolation Kit (Applied Biosystems, Foster City, California) following the manufacturer's instructions and quantified by the NanoDrop ND-2000 (Thermo Scientific Inc., Waltham, Massachusetts). The RNA integrity was assessed using Agilent Bioanalyzer 2100 (Agilent Technologies).

The PrimeScript RT reagent Kit (Perfect Real Time) (TAKARA, Otsu, Japan) was used to synthesize the first-strand cDNA according to the manufacturer's instructions. The SYBR Green real-time PCR (RT-PCR) assay kit (TAKARA) was used for amplification of cDNA. The mRNA levels of SLC6A13, USP31, GADD45B, ATF3, SH3MD1, FANCF, and the internal standard GAPDH were measured by qRT-PCR in triplicates using a 7500 RT-PCR system (Applied Biosystems). Primers specific to the above genes are listed in Table 1.

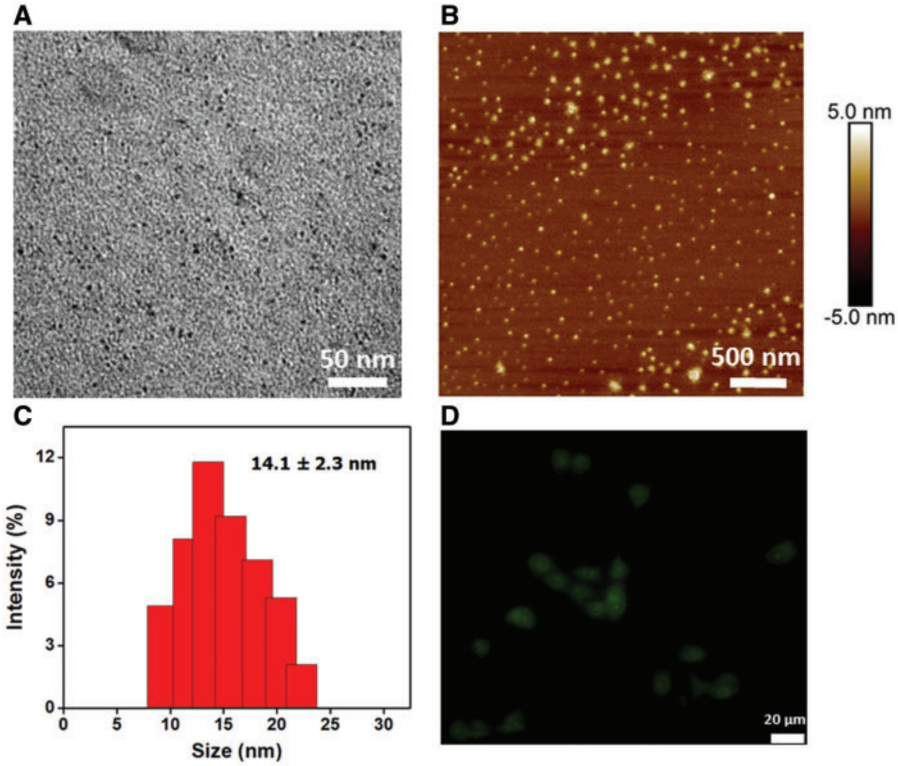

Figure 1. Characterization of OH-GQDs nanoparticles. A, TEM image of OH-GQDs. Scale bar = 50 nm. B, AFM image of OH-GQDs. Scale bar = 500 nm. C, Hydrodynamic size of OH-GQDs in deionied water. D, Fluorescence image of HET-1A cells after treatment with OH-GQDs for 24 h. Scale bar = 20 μm. (For interpretation of the references to colour in this figure legend, the reader is referred to the web version of this article.)

Statistical analysis. The data are presented as the mean ± SD of 3 independent experiments. Statistical analyses were conducted using SPSS 16.0 software (SPSS Inc., Chicago, Illinois). Student's t test was used for 2-group comparison and one-way ANOVA was performed for multiple comparisons. All tests were 2-sided and differences were considered significant when $p < .05$.

RESULTS

OH-GQDs Characterization

TEM imaging of the OH-GQDs (Figure 1A) showed that they range in size from 4 to 6 nm. Figure 1B illustrates the topographic morphology of OH-GQDs as characterized by AFM; the heights are mainly distributed between 1 and 3 nm. The DLS analysis showed that OH-GQDs in deionied water had a narrow size distribution with an average hydrodynamic size of 14.1 ± 2.3 nm (Figure 1C). To study the cellular uptake of OH-GQDs, fluorescence microscope was used to assess the cellular uptake of OH-GQDs. The results showed that OH-GQDs can be efficiently uptaken by esophageal epithelial cells HET-1A (Figure 1D). We further detected the internalized OH-GQDs by flow cytometry. The SSC is proportional to cell granularity or internal complexity, thus any nanoparticles within the cells will result in the changing in the SSC signals. The SSC signals in cells treated with OH-GQDs were shown in Supplementary Figure 1. A significantly increased SSC signal was detected in OH-GQDs-treated cells when compared with control cells, indicating that OH-GQDs entered into cells efficiently.

OH-GQDs Inhibited Cellular Viability and Arrested Cell Cycle Progression of Human Esophageal Epithelial Cells

Since oral administration is a preferred mode of drug delivery in humans, an esophageal epithelial cell line (HET-1A) was used as a model to assess the potential cytotoxicity of OH-GQDs. The HET-1A cells were exposed to different concentrations (25–200 μg/ml) of OH-GQDs for 24 and 48 h. As shown in Figures 2A and 2B, OH-GQDs significantly reduced the cell proliferation in a dose- and time-dependent manner. When compared with the untreated group, the viability of HET-1A cells was decreased to 13% and 2% after treated with 100 and 200 μg/ml OH-GQDs respectively for 24 h (Figure 2A). As shown in Figure 2B, 100 and 200 μg/ml OH-GQDs killed almost all the cells after 48-h treatment. We also found that OH-GQDs exhibited obvious cellular toxicity on normal human hepatic cells LO2, human small intestine epithelium cells HIEC-6 and human esophageal cancer cells ECA-109 (Supplementary Figures. 2 and 5A).

To further determine the effect of OH-GQDs on proliferation, the cell cycle progression of HET-1A cells was detected by flow cytometry. The HET-1A cells were incubated with 25 and 50 μg/ml OH-GQDs for 24 and 48 h. As shown in Figures 2C and 2D, OH-GQDs significantly induced G_0/G_1 phase arrest in HET-1A cells. The percentage of cells blocked in G_0/G_1 phase increased from 57.2% in the untreated group to 68.78% and 80.83% in the groups treated with 25 and 50 μg/ml OH-GQDs for 24 h, respectively. The percentage of G_0/G_1 arrested cells increased from 57.7% in control group to 82.02% and 89.16% in the groups treated with 25 and 50 μg/ml OH-GQDs for 48 h, respectively. However, the Annexin V-FITC-staining assays revealed that OH-GQDs significantly induced apoptosis only at the high OH-GQDs dose (100 μg/ml) but not at moderate dose (25 and 50 μg/ml) in HET-1A cells (Supplementary Figure 3).

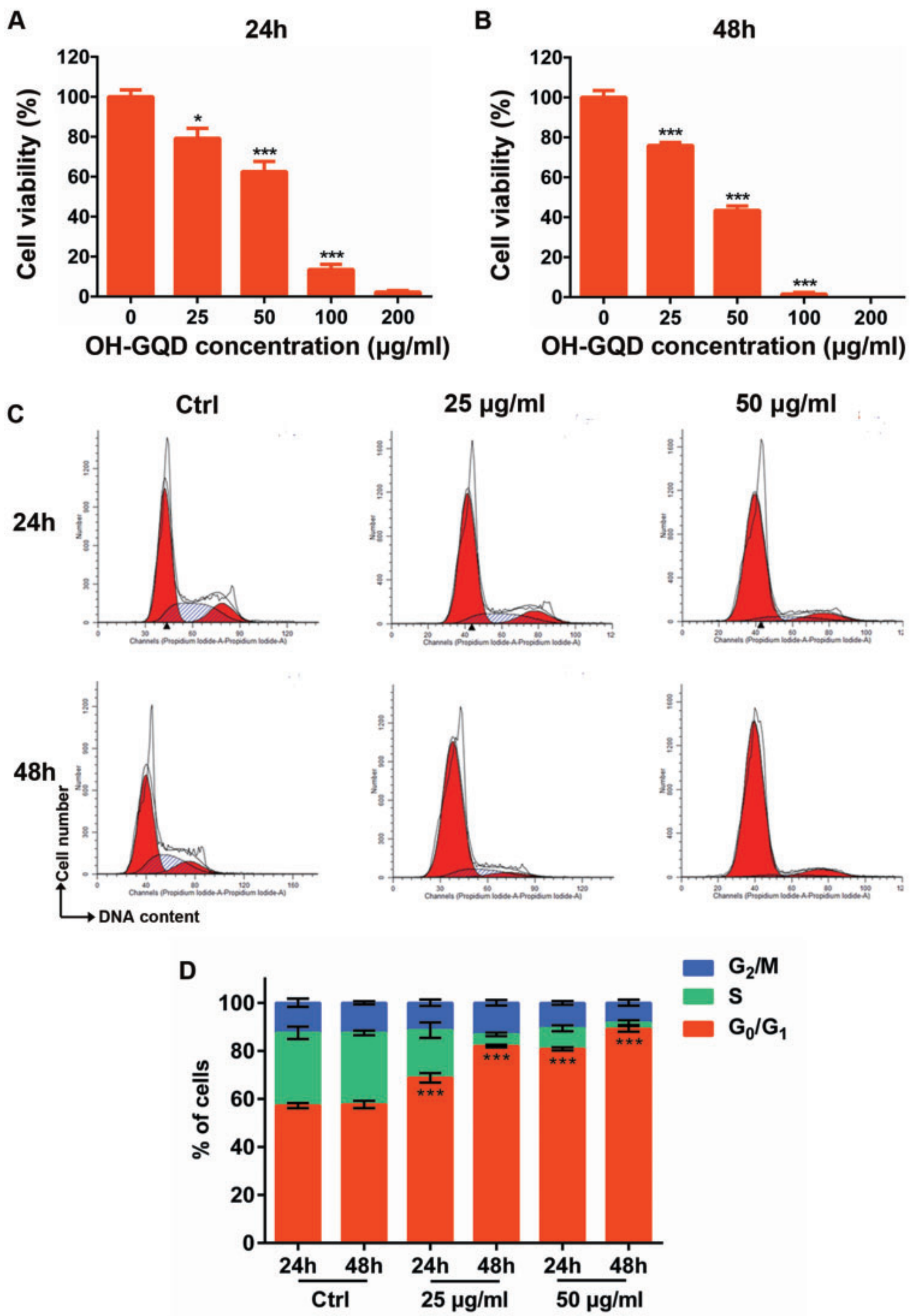

Figure 2. The cytotoxicity of OH-GQDs and their effects on cell cycle distribution. (A and B) Cell viability after exposure to indicated concentration of OH-GQDs (0, 25, 50, 100, and 200 μg/ml) for 24 and 48 h, respectively. One-way ANOVA was performed and data are presented as mean ± SD, $n = 5$. When compared with 0 μg/ml OH-GQDs-treated cells, $^{*}p < .05$, $^{**}p < .01$, $^{***}p < .001$. (C and D) HET-1A cells were exposed to 25 and 50 μg/ml OH-GQDs for 24 or 48 h and cell cycle distribution was analyzed by flow cytometry. One-way ANOVA was performed. The data are presented as the mean ± SD from 3 tests. When compared with the control cells which were harvested at the same time point, *** $p < .001$.

The OH-GQDs-Induced DNA Damage and Increased Genomic Instability in HET-1A Cells

Our previous data demonstrated that OH-GQDs activated the p53 signaling pathway in the human nonsmall cell lung cancer cell line A549 (Tian *et al*., 2016). The p53 protein has long been recognized as the guardian of the genome as it mediates cell cycle arrest, DNA repair and cell death in response to DNA damage. However, the precise effects of OH-GQDs on genomic stability have not been fully clarified. As one of the variants of core histone H2A, H2AX has a unique C-terminal extension carrying a conserved serine residue (Ser139) which is phosphorylated in response to DNA damage. The phosphorylated H2AX (γ-H2AX) at the damaged sites is a docking platform for further recruitment of DNA damage repair factors. The phosphorylated

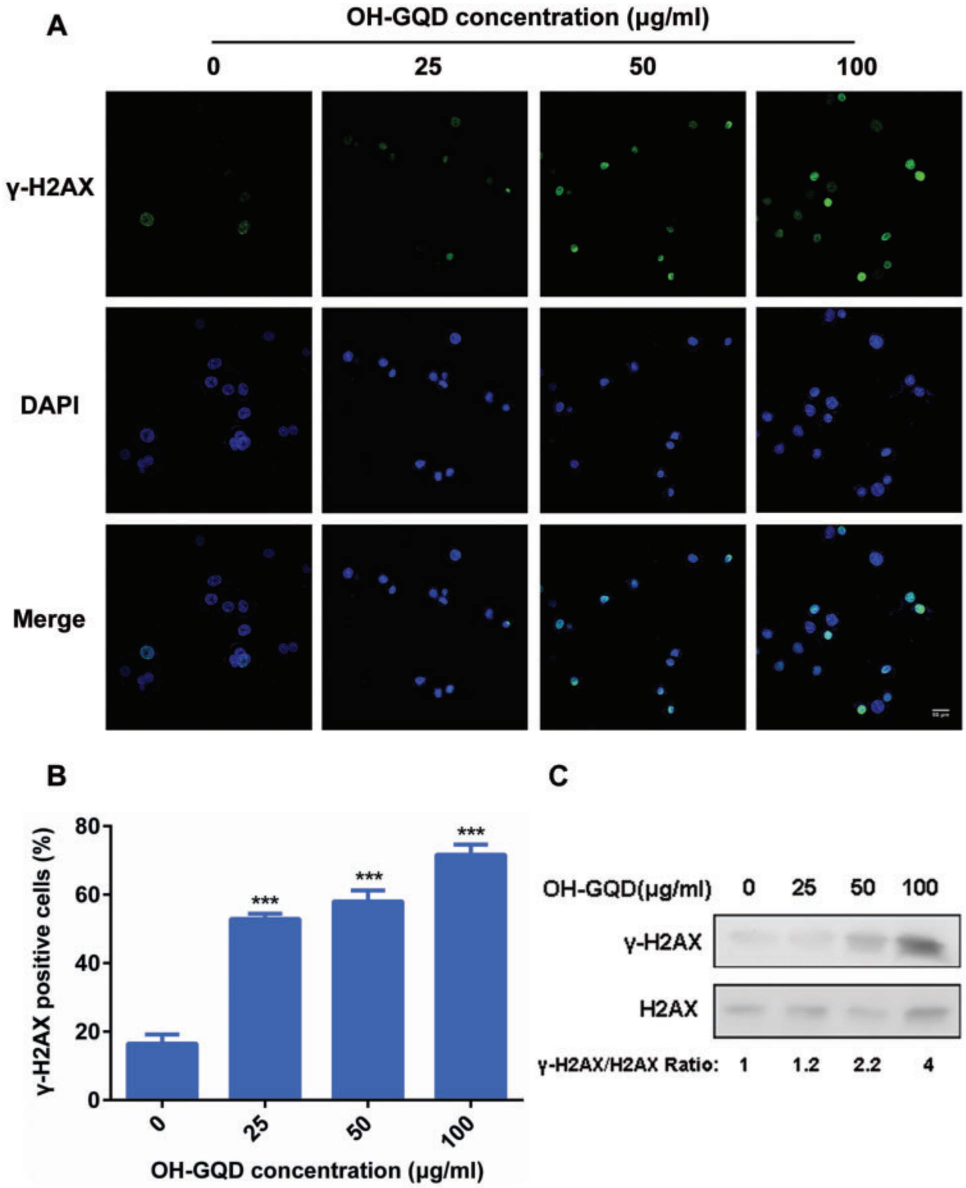

Figure 3. OH-GQDs induced DNA damage in human esophageal epithelial cells. A, HET-1A cells were treated with the indicated concentration (0, 25, 50, and 100 μg/ml) of OH-GQDs for 24 h; samples were collected and immuno-stained for anti-γ-H2AX antibody. The incidences of γ-H2AX-positive cells were counted. Scale bar = 50 μm. B, Quantitative data are represented as mean ± SD from 3 tests. One-way ANOVA was performed. When compared with 0 μg/ml OH-GQDs-treated cells, *** $p < .001$. C, Western blot analysis for γ-H2AX and H2AX expressions between OH-GQDs treated and control cells. (For interpretation of the references to colour in this figure legend, the reader is referred to the web version of this article.)

signal can be detected by immunofluorescent staining and provides a convenient method to assess the number of DNA lesions. In this study, we used this assay to monitor DNA damage in the HET-1A cells exposed to different concentrations of OH-GQDs for 24 h (Figure 3A). The results showed that the percentage of γ-H2AX positive cells increased from 16% to 53%, 58% and 73% following treatment with 25, 50, and 100 μg/ml OH-GQDs, respectively (Figure 3B). We further determined the expression levels of γ-H2AX and H2AX in HET-1A cells treated with different doses of OH-GQDs using Western blot. As shown in Figure 3C, OH-GQDs promote H2AX phosphorylation in a dose-dependent manner.

The cytokinesis-blocked micronucleus assay is another frequently used method to measure DNA lesions—precisely the damaged chromosomes fragments that fail to bind to the mitotic spindle and lag behind during nuclear separation. In addition, this assay can also detect nucleoplasmic bridges generating from asymmetrical chromosome rearrangements and nuclear buds which represent gene amplification. As shown in Figure 4, the abnormal nuclei frequency increased significantly only at the high OH-GQDs dose (100 μg/ml). Although the frequency of micronucleus increased from 11% to 19%, OH-GQDs did not induce the generation of nucleoplasmic bridges and nuclear buds in HET-1A cells. These data provide direct evidence that OH-GQDs nanoparticles induce DNA damage and increase genomic instability in human esophageal epithelial cells. Oxidative stress is one of the most common reasons leading to DNA damage. Consistent with this, we observed that OH-GQDs dramatically promote the generation of ROS in HET-1A cells in a dose- and time-dependent manner (Supplementary Figure 4).

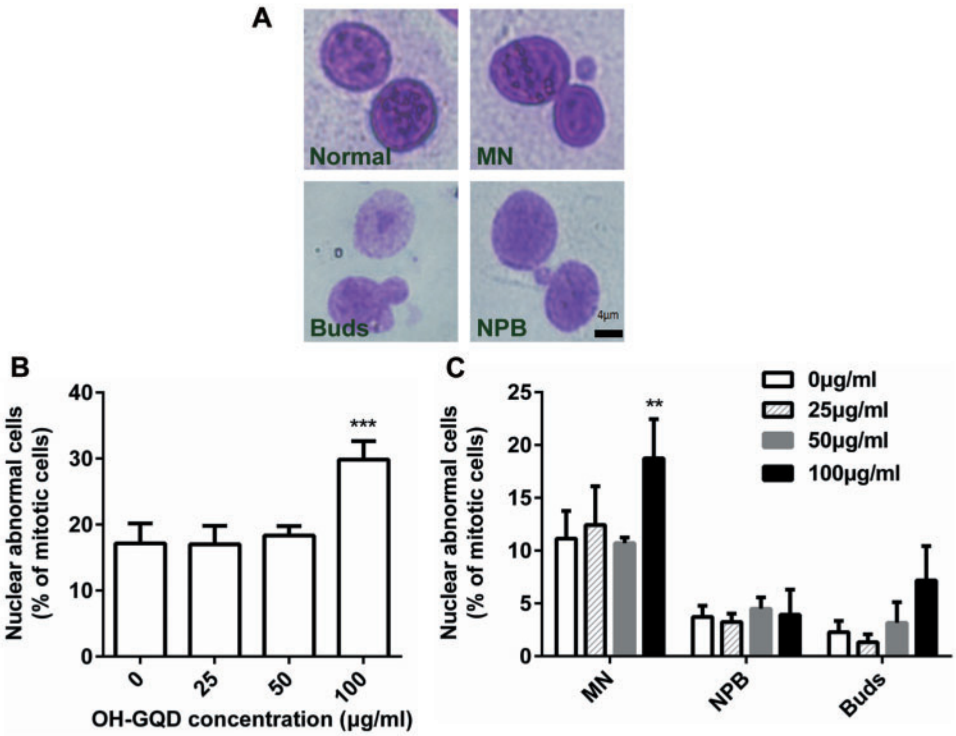

Figure 4. Cytokinesis-blocked micronucleus formation in HET-1A cells exposed to OH-GQDs. A, Representative images of cells scored using the cytokinesis-blocked micronuleus assay: Normal cell, binucleated cell with micronucleus (MN), binucleated cell with buds (Buds) and binucleated cell with nucleoplasmic bridge (NPB). Scale bar = 4 μm. B, The percentage of nuclear abnormal cells in mitotic cells were counted and represented as mean ± SD from 3 tests. One-way ANOVA was performed. When compared with 0 μg/ml OH-GQDs-treated cells, *** $p < .001$. C, The percentage of nuclear abnormal cells with MN, NPB, and Buds in mitotic cells were counted separately and represented as mean ± SD. One-way ANOVA was performed. When compared with 0 μg/ml OH-GQDs-treated cells, **$p < .01$.

OH-GQDs Interfered With Multiple Signaling Pathways and Decreased the Expression Levels of a Number of Genes Involved in DNA Damage Response and Cell Cycle Progression

To understand the potential molecular mechanism through which OH-GQDs disrupted cell cycle progression and induced DNA damage, the gene expression profiles of OH-GQDs-treated and -untreated HET-1A cells were evaluated and compared using microarray. HET-1A cells were harvested 24 h postculture with or without 50 μg/ml OH-GQDs and processed for microarray. The data revealed that 8151 genes had a 2-fold or higher change in expression level in the OH-GQDs-treated compared with the untreated cells. Among them, 3895 genes were up-regulated and 4256 genes were down-regulated (Figures. 5A and 5B). The top 20 genes dysregulated in the OH-GQDs-treated cells in comparison to the vehicle-treated cells are shown in Tables 2 and 3. Pathway analysis showed that OH-GQDs treatment specifically altered the expression of genes associated with several key DNA damage response signaling pathways, including Fanconi anemia (FA), homologous recombination (HR) repair, mismatch repair, base excision repair, cell cycle, DNA replication, and p53 signal pathways (Figures. 5C and 5D). The expression levels of 6 representative genes were validated by qRT-PCR and that of FANCF, SH3MD1, USP31, ATF3, and GADD45B were consistent with microarray data (Figure 5E).

The FA DNA damage repair pathway plays a crucial role in repairing DNA inter-strand crosslinks (ICLs) and is also reported to participate in replication stress response and HR. Our data revealed that OH-GQDs decreased the expression of a number of genes in FA and HR pathways, including the essential factor FANCD2 (Figures. 6A and 6B). We further validated the protein level of FANCD2 in HET-1A cells treated with different doses of OH-GQDs using Western blot. As shown in Figure 6C, OH-GQDs inhibited FANCD2 protein expression in a dose-dependent manner. In addition, OH-GQDs also suppressed the expression of DNA-PKcs and ATM in both normal esophageal epithelial cells HET-1A (Figure 6C) and esophageal cancer cells ECA-109 (Supplementary Figure 5B), which are key regulators of DNA double-strand breaks (DSBs) repair pathway.

Our study revealed that OH-GQDs lead to cell cycle arrest, consistent with altered expression patterns of many cell cycle-related genes in response to OH-GQDs treatment (Figure 6D) which was also validated by Western blotting data (Figure 6E).

OH-GQDs Inhibited the Expression of Microtubule-Associated Proteins, Disrupted Microtubule Integrity and Interfered With Microtubule Regrowth

Microtubule-associated proteins (MAPs) can bind to the microtubules and regulate their organization. Microarray data revealed that OH-GQDs inhibited the expression of MAPs genes (Figure 7A). To investigate the effect of OH-GQDs on microtubule functions, the microtubules in HET-1A cells were visualized by immuno-staining against α-tubulin which was detected using confocal immunofluorescence microscopy. As shown in Figure 7B, 25 μg/ml OH-GQDs was enough to disrupt microtubules as early as 24 h and a higher dose (100 μg/ml) could completely disrupt the microtubule structure and lead to their dissolution. To further assess the involvement of OH-GQDs in microtubule dynamics, OH-GQDs treated or control HET-1A cells were exposed to nocodazole in chilled medium to

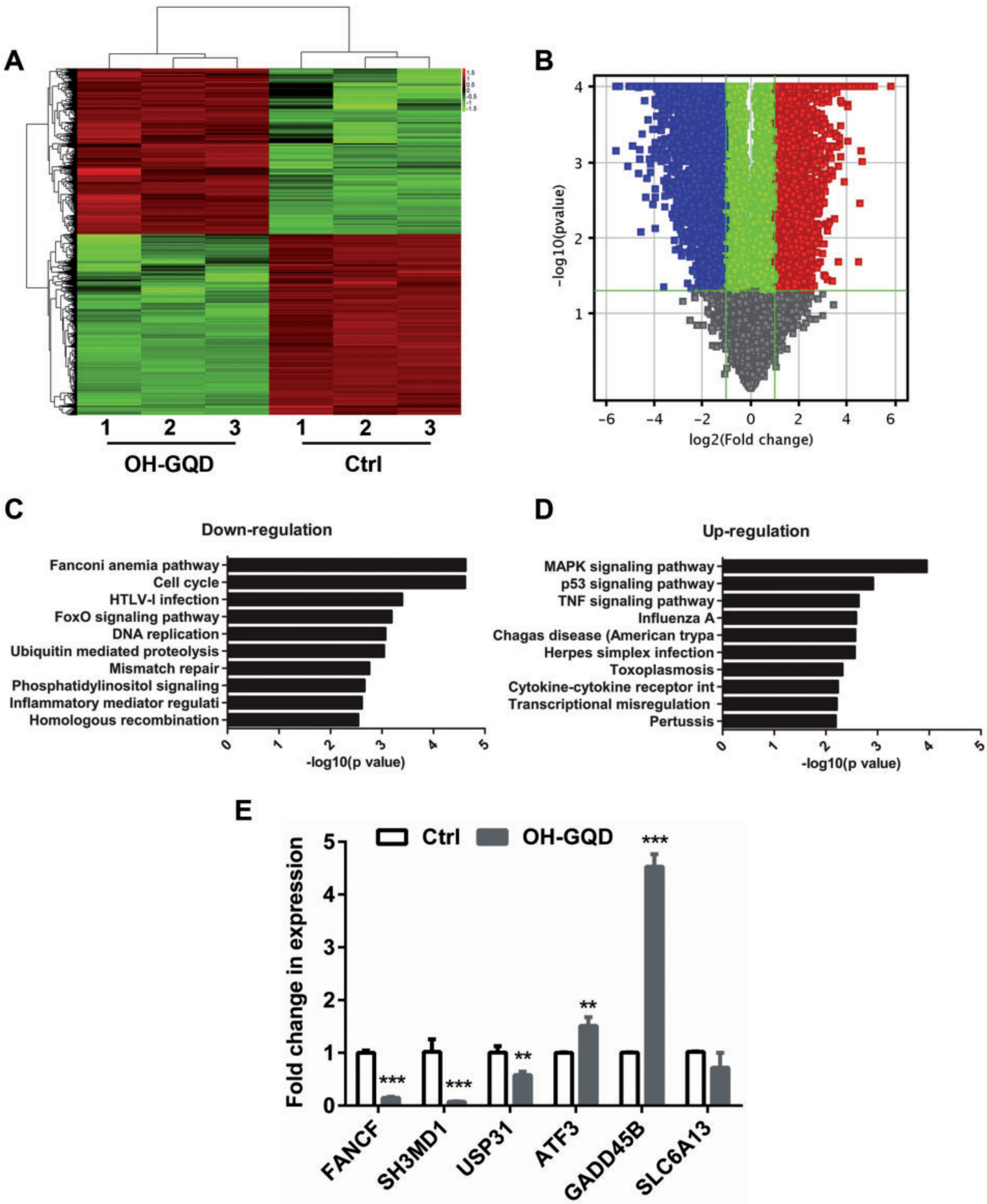

Figure 5. Significant pathways altered in OH-GQDs-treated human esophageal epithelial cells. A, Clustering map of genes differentially expressed in OH-GQDs-treated and control HET-1A cells. B, Volcano plot comparing vehicle treatment versus OH-GQDs treatment. C and D, Significant pathways altered in OH-GQDs treated and control HET-1A cells. E, Quantitative real-time PCR validation for selected genes between OH-GQDs treated and control cells ($n = 3$). Student's t test was performed. When compared with control cells, $^{**}p < .01$, $^{***}p < .001$. (For interpretation of the references to colour in this figure legend, the reader is referred to the web version of this article.)

depolymerize the microtubules. Once nocadazole was removed and the medium changed to prewarmed RPMI-1640 with 25 and 50 μg/ml OH-GQDs, the microtubules started to regrow. The area of the nucleated microtubules around centrosomes was analyzed in OH-GQDs treated and control cells which showed that microtubule growth was significantly slowed down in the

Table 2. Top 20 Genes Upregulated Within OH-GQDs- and Vehicle-Treated HET-1A Cells (OH-GQDs-Treated versus Vehicle-Treated Cells)

Gene Name	Fold Change Upregulated	*P*-Value	Chromosome	Definition
SLC6A13	56.18	5.29E-05	chr12	Solute carrier family 6 (neurotransmitter transporter), member 13
ATF3	35.58	9.44E-07	chr1	Activating transcription factor 3
HMOX1	30.29	1.32E-06	chr22	Heme oxygenase (decycling) 1
RSAD2	30.06	2.75E-05	chr2	Radical S-adenosyl methionine domain containing 2
IL10RA	26.34	8.14E-06	chr11	Interleukin 10 receptor, alpha
FRZB	26.18	2.18E-05	chr2	Frizzled-related protein
PLCB1	24.94	9.95E-06	chr20	Phospholipase C, beta 1 (phosphoinositide-specific)
AOC3	24.72	9.85E-04	chr17	Amine oxidase, copper containing 3
EGR4	24.38	3.61E-06	chr2	Early growth response 4
MAFB	23.92	5.57E-07	chr20	V-maf avian musculoaponeurotic fibrosarcoma oncogene homolog B
COL20A1	23.7	7.12E-04	chr20	Collagen, type XX, alpha 1
JUN	23.39	1.30E-06	chr1	Jun proto-oncogene
LIPN	22.56	2.10E-02	chr10	Lipase, family member N
PYGM	21.37	8.08E-05	chr11	Phosphorylase, glycogen, muscle
CTGF	21.29	8.22E-07	chr6	Connective tissue growth factor
GADD45G	20.76	6.35E-09	chr9	Growth arrest and DNA-damage-inducible, gamma
CDRT1	20.46	1.91E-05	chr17	CMT1A duplicated region transcript 1
OASL	18.04	2.64E-06	chr12	2′-5′-oligoadenylate synthetase-like
ANKRD1	17.65	5.55E-06	chr10	Ankyrin repeat domain 1 (cardiac muscle)
FAM71F1	16.84	4.91E-06	chr7	Family with sequence similarity 71, member F1

Table 3. Top 20 Genes Downregulated Within OH-GQDs- and Vehicle-Treated HET-1A cells (OH-GQDs-Treated Versus Vehicle-Treated Cells)

Gene Name	Fold Change Downregulated	*P*-Value	Chromosome	Definition
ADAT2	47.67	4.12E-06	chr6	Adenosine deaminase, tRNA-specific 2
CSF3	42.88	7.14E-05	chr17	Colony stimulating factor 3 (granulocyte)
TMEM71	34.1	1.13E-03	chr8	Transmembrane protein 71
SH3PXD2A	32.61	1.23E-07	chr10	SH3 and PX domains 2A
PSD3	26.61	1.08E-05	chr8	Pleckstrin and Sec7 domain containing 3
USP31	26.19	3.02E-05	chr16	Ubiquitin-specific peptidase 31
PPARGC1B	24.6	1.02E-04	chr5	Peroxisome proliferator-activated receptor gamma, coactivator 1 beta
SH3PXD2A	23.95	9.04E-04	chr10	SH3 and PX domains 2A
U2SURP	23.37	9.82E-05	chr3	U2 snRNP-associated SURP domain containing
ADARB2	22.96	8.61E-03	chr10	Adenosine deaminase, RNA-specific, B2 (nonfunctional)
RNF207	20.34	8.34E-06	chr1	Ring finger protein 207
B4GALNT4	20.17	2.94E-03	chr11	Beta-1, 4-N-acetyl-galactosaminyl transferase 4
FAM208A	19.91	6.38E-06	chr3	Family with sequence similarity 208, member A
NMNAT3	18.59	2.69E-04	chr3	Nicotinamide nucleotide adenylyltransferase 3
CA12	17.77	1.38E-03	chr15	Carbonic anhydrase XII
PAQR5	17.54	1.05E-03	chr15	Progestin and adipoQ receptor family member V
C1orf21	17.3	7.06E-07	chr1	Chromosome 1 open reading frame 21
MPRIP	16.96	2.17E-05	chr17	Myosin phosphatase Rho interacting protein
TRAF5	16.73	3.61E-03	chr1	TNF receptor-associated factor 5
SRGAP3	15.53	7.99E-04	chr3	SLIT-ROBO Rho GTPase activating protein 3

OH-GQDs-treated cells (Figures. 7C and 7D). These results thus reveal a novel function of OH-GQDs in microtubule dynamic regulation.

DISSCUSSION

Several recent studies have demonstrated that carbon nanomaterials could activate the DNA damage response by enhancing the expression of p53, ATM, and Rad51 (Liu *et al.*, 2013; Wang *et al.*, 2015). Our current work showed that OH-GQDs significantly increased the phosphorylation of H2AX at its Ser139 and increased the number of micronucleus in the human esophageal epithelial cell line HET-1A (Figures. 3 and 4). Our and others' previous investigations revealed that GQDs triggered the generation of ROS (Qin *et al.*, 2015; Tian *et al.*, 2016), which play key roles in mediating physical and chemical agents induced DNA damage (Cooke *et al.*, 2003). To further understand the molecular mechanism of OH-GQDs-mediated DNA damage response, gene expression analysis was done using mRNA microarray which identified 3895 up-regulated and 4256 down-regulated genes. Among them, the genes associated with several key DNA damage response signaling pathways, including FA, HR, mismatch

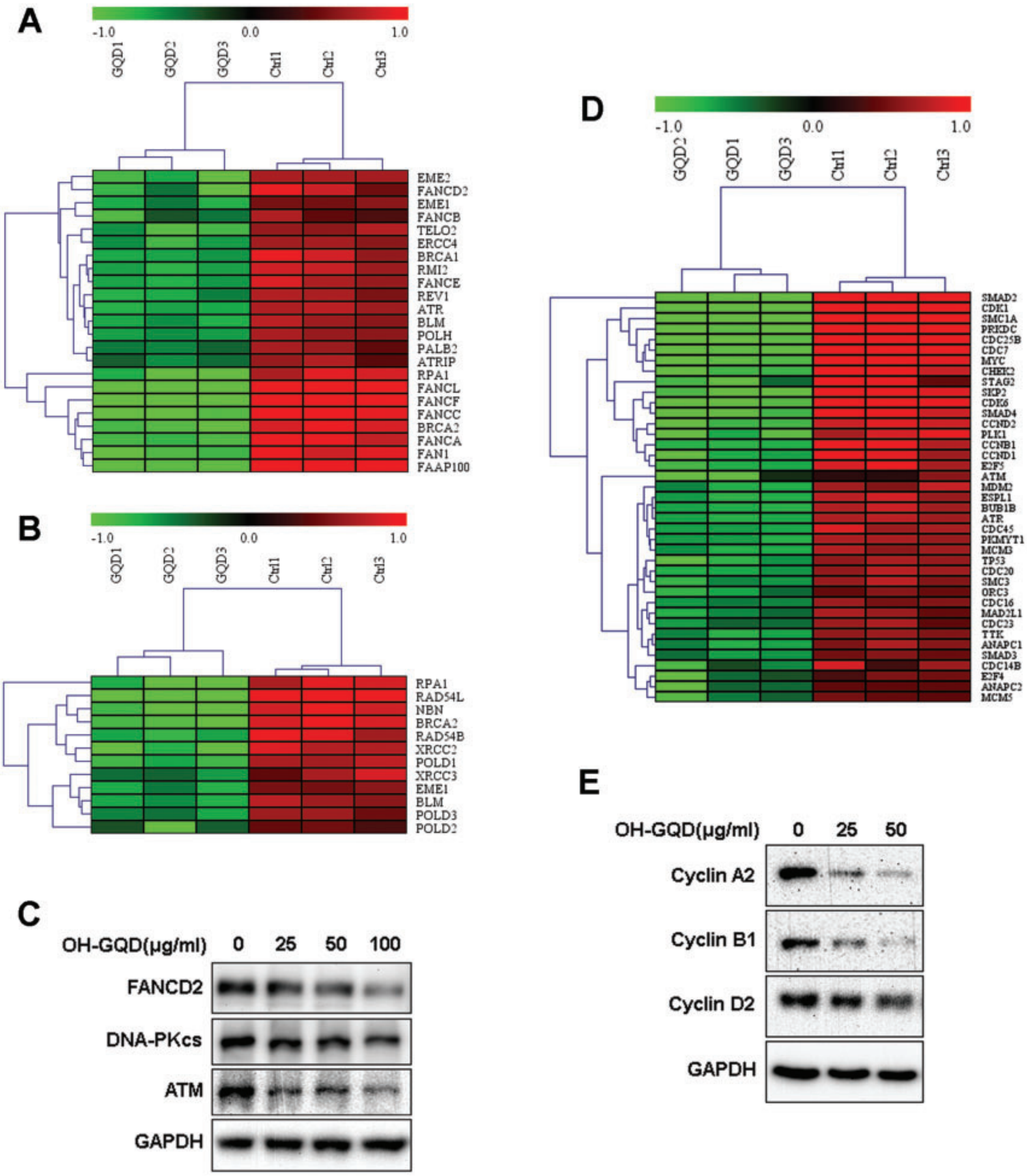

Figure 6. Heat maps and validation of differentially expressed genes related to DNA damage repair and cell cycle regulation in response to OH-GQDs treatment. The expression of (A) FA pathway genes, (B) HR repair genes, and (D) DNA DSBs response and cell cycle regulation pathway genes in OH-GQDs treated and control cells. C and E, Western blot validation for differentially expressed proteins between OH-GQDs treated and control cells.

repair, base excision repair (Figures. 5C and 5D). The DNA DSBs are among the most toxic types of DNA lesions and DNA DSBs response signaling pathways are coordinated by 3 phosphatidylinositol 3-kinase-like family members: ATM, DNA-PKcs, and ataxia telangiectasia and Rad3-related (ATR) (Marechal and Zou, 2013). In response to DNA damage, ATM is immediately activated and participates in both nonhomologous end joining (NHEJ) and HR pathways and cell cycle checkpoint response (Lee and Paull, 2005). DNA-PKcs mainly contributes to DNA repair through NHEJ pathway (Davis and Chen, 2013), whereas ATR is activated by the generation of signal-stranded DNA by DNA damage end resection (Cimprich and Cortez, 2008). It has been reported that lots of small molecular compounds target different DNA damage repair proteins. For example, Shamanna *et al.* (2016) found that camptothecin, a inhibitor of DNA topoisomerase I (Top1), promotes WRN degradation in ubiquitin-proteasome dependent manner. Yan *et al.* (2006) revealed that vanillin derivate bromovanin induces cleavage of DNA-PKcs. In addition, DNA-PKcs is subject to cleavage by proteases during apoptosis (McConnell *et al.*, 1997). However, our study showed that the mRNA levels of several DNA repair genes, such as ATM and DNA-PKcs, were dramatically down-regulated in OH-GQDs-treated cells (Figure 6C). How the nanoparticles affect the transcription of DNA damage response proteins is still unclear. Interestingly, a recent investigation demonstrated that heat shock-induced activation of endoplasmic reticulum (ER) stress inhibits transcription of several DNA repair proteins via ATF4 and IRE1α (Zhu *et al.*, 2012). Pagliarini *et al.* (2015) identified that transcription factors E2F1 is also down-regulated during

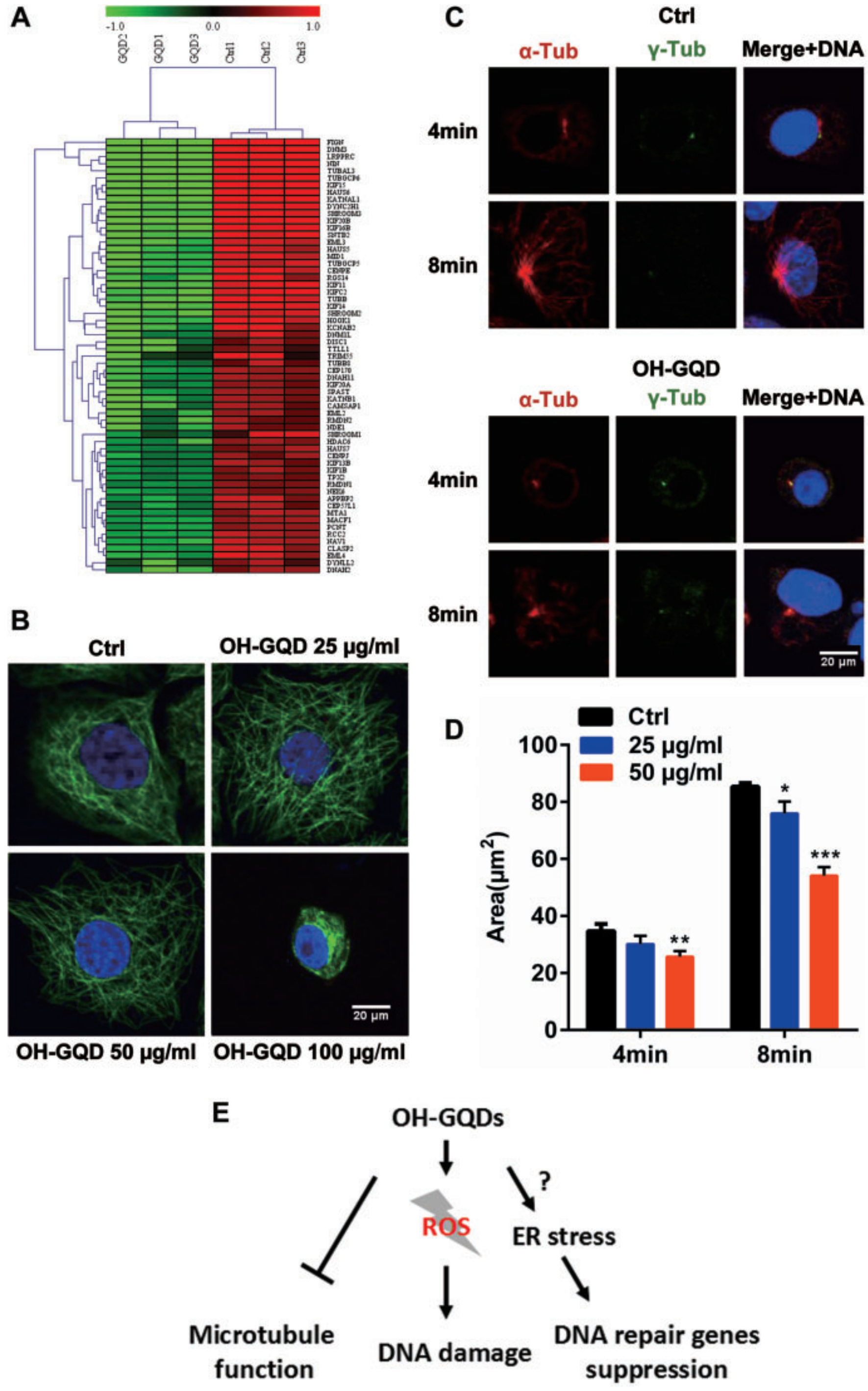

Figure 7. OH-GQDs treatment disrupted microtubule structure and suppressed microtubule regrowth around centrosomes. A, Differentially expressed genes related to tubulin functions in response to OH-GQDs treatment. B, HET-1A cells were exposed to the indicated concentration (0, 25, 50, and 100 μg/ml) of OH-GQDs for 24 h. Cells were fixed and stained with anti-α-tubulin antibody to visualize microtubules (green) and DAPI to visualize the nucleus (blue). Scale bar = 20 μm. C, The HET-1A cells were treated with chilled medium + 1 μg/ml nocodazole for 1 h on the ice. Microtubule nucleation and regrowth were detected at the indicated time post nocodazole removal in 25 and 50 μg/ml OH-GQDs treated and control cells. Scale bar = 20 μm. D, The area of microtubule around the centrosomes was measured and quantitative data are represented as mean ± SD from 3 tests ($n \geq 50$). One-way ANOVA was performed. When compared with control cells, $^{*}p < .05$, $^{**}p < .01$, $^{***}p < .001$. E, The OH-GQDs exhibit significant cytotoxic effects via increasing DNA damage, suppressing the expression of DNA damage repair genes and disturbing microtubule function. (For interpretation of the references to colour in this figure legend, the reader is referred to the web version of this article.)

ER stress-induced apoptosis. It is well known that E2F1 is an upstream transcriptional factor for lots of DNA repair genes, such as BRCA1, RAD51, and RAD52 (Wang *et al.*, 2016). Therefore, it will be interesting to further determine whether OH-GQDs trigger ER stress and inhibit DNA repair genes expression via E2F1 in the next study (Figure 7E).

OH-GQDs also inhibited the expression of several genes involved in the FA pathway which plays a central role in repairing

DNA ICLs and maintaining genome stability (Moldovan and D'Andrea 2009). To date, 18 gene products (FANCA to FANCT) have been identified in the FA pathway. A germline mutation in any one of these genes leads to the FA syndrome, a rare human genetic disease that causes bone marrow failure and results in a high incidence of tumorigenesis (Schwab *et al.*, 2015). In addition to its function in repairing ICL lesions, FA pathway also participates in replication fork maintenance and the regulation of DNA DSBs end resection (Michl *et al.*, 2016; Moldovan and D'Andrea 2009). Based on the microarray data, at least 9 of the FA pathway members were downregulated in OH-GQDs-treated HET-1A cells (Figure 6A). In addition, the expression of genes related to HR, mismatch repair and base excision repair was also significantly decreased in response to OH-GQDs treatment. Several previous studies have shown that GQDs induce oxidative stress which activates DNA damage response (Qin *et al.*, 2015; Tian *et al.*, 2016; Wang *et al.*, 2015). Our results confirmed that OH-GQDs suppressed the expression of many important DNA damage repair genes which might further enhance ROS-induced genotoxicity (Figure 7E). Consistent with this, we observed that OH-GQDs dramatically induced DNA damage and increased the genomic instability in HET-1A cells. It is widely accepted that chemical or occupational (such as silica and asbestos) toxicant exposure is one of the major reasons leading to the esophageal cancer (Kamangar *et al.*, 2009). The increased genomic instability is hallmark of most human cancer and plays an important role in tumor development (Hu *et al.*, 2009). Here, our data indicated that OH-GQDs have the potential risk to contribute to esophageal carcinogenesis via inducing DNA damage and increasing genomic instability in human esophageal epithelial cells. However, although the genotoxicity of OH-GQDs limits its general biomedical application, it can actually prove to be advantageous in cancer therapy. Since DNA damage is a significant cause of radio- and chemotherapy-induced cell death in different types of cancer cells, targeting the DNA damage repair system is one of the most common strategies used to sensitize the tumors to radio- and chemotherapy (Begg *et al.*, 2011). The surface of OH-GQDs can be suitably modified to enhance its targeted delivery to cancer cells where it can specifically block the DNA damage repair system.

When associated with their corresponding partner cyclins, cyclin-dependent kinases (CDKs) can be activated and promote cell cycle progression by phosphorylating appropriate substrates (Malumbres and Barbacid, 2009). We found that several cyclins and CDKs were down-regulated in OH-GQDs-treated cells, which was consistent with the G_0/G_1 cell cycle arrest induced by OH-GQDs. In addition, our data also revealed that OH-GQDs inhibited expression of many tubulin and MAPs genes. Microtubules are key components of the cytoskeletal system and play an important role in cell shape maintenance, mobility, and division (Pasquier and Kavallaris, 2008). Our study showed that OH-GQDs prevented microtubules assembly and disrupted their structure within cells. To date, several investigations have revealed that disruption of cytoskeletal structures can be induced by different kinds of nanoparticles (Holt *et al.*, 2010; Ratnikova *et al.*, 2011; Tian *et al.*, 2017). For instance, Tian *et al.* (2017) found that GO can directly interact with and disrupt intracellular actin filaments while Ratnikova *et al.* (2011) reported that the nanoparticle C(60)(OH)(20) forms hydrogen bonds with tubulin heterodimer and inhibits microtubule polymerization. In this study, we only treated cells with OH-GQDs for very short time (only several minutes), but it is already enough to affect microtubule assembly speed. We speculate that there might be some more direct association between OH-GQDs and microtubule. Further studies will be focused on exploring whether OH-GQDs directly interact with the cytoskeletal system. More importantly, a recent study demonstrated that microtubules play an important role in mediating trafficking of DNA damage proteins (Poruchynsky *et al.*, 2015). Therefore, the disruption of cytoskeleton system by OH-GQDs might further enhance their genotoxic effects via interfering with DNA repair proteins' transport in cells.

In conclusion, we explored the biological effects of OH-GQDs in human esophageal epithelial cells and found that OH-GQDs can induce cell cycle arrest, DNA damage and increase genomic instability. Microarray analysis demonstrated that OH-GQDs inhibit the expression of genes associated with multiple signaling pathways such as DNA damage repair, cell cycle progression and cytoskeleton maintenance (Figure 7E).

SUPPLEMENTARY DATA

Supplementary data are available at *Toxicological Sciences* online.

FUNDING

This work was supported by the Priority Academic Program Development of Jiangsu Higher Education Institutions (PAPD), Jiangsu Provincial Key Laboratory of Radiation Medicine and Protection and the National Natural Science Foundation of China (grant numbers 81530085, 81573079, 81472919, and 81673091).

ACKNOWLEDGMENTS

We thank Dr Jundong Zhou for providing the cell line HET-1A.

REFERENCES

Abdullah-Al-Nahain, L.,J. E., In, I., Lee, H., Lee, K. D., Jeong, J. H., and Park, S. Y. (2013). Target delivery and cell imaging using hyaluronic acid-functionalized graphene quantum dots. *Mol. Pharm.* **10**, 3736–3744.

Begg, A. C., Stewart, F. A., and Vens, C. (2011). Genomic instability in cancer strategies to improve radiotherapy with targeted drugs. *Nat. Rev. Cancer* **11**, 239–253.

Chong, Y., Ma, Y. F., Shen, H., Tu, X. L., Zhou, X., Xu, J. Y., Dai, J. W., Fan, S. J., and Zhang, Z. J. (2014). The in vitro and in vivo toxicity of graphene quantum dots. *Biomaterials* **35**, 5041–5048.

Cimprich, K. A., and Cortez, D. (2008). ATR: An essential regulator of genome integrity. *Nat. Rev. Mol. Cell Biol.* **9**, 616–627.

Cooke, M. S., Evans, M. D., Dizdaroglu, M., and Lunec, J. (2003). Oxidative DNA damage: Mechanisms, mutation, and disease. *Faseb J.* **17**, 1195–1214.

Davis, A. J., and Chen, D. J. (2013). DNA double strand break repair via non-homologous end-joining. *Transl. Cancer Res.* **2**, 130–143.

Ge, J. C., Lan, M. H., Zhou, B. J., Liu, W. M., Guo, L., Wang, H., Jia, Q. Y., Niu, G. L., Huang, X., Zhou, H. Y., *et al.*, (2014). A graphene quantum dot photodynamic therapy agent with high singlet oxygen generation. *Nat. Commun.* **5**,

Holt, B. D., Short, P. A., Rape, A. D., Wang, Y. L., Islam, M. F., and Dahl, K. N. (2010). Carbon nanotubes reorganize actin structures in cells and ex vivo. *Acs Nano* **4**, 4872–4878.

Hu, N., Wang, C., Ng, D., Clifford, R., Yang, H. H., Tang, Z. Z., Wang, Q. H., Han, X. Y., Giffen, C., Goldstein, A. M., *et al.* (2009). Genomic characterization of esophageal squamous cell carcinoma from a high-risk population in China. *Cancer Res.* **69**, 5908–5917.

Jiang, D., Chen, Y. P., Li, N., Li, W., Wang, Z. G., Zhu, J. L., Zhang, H., Liu, B., and Xu, S. (2015). Synthesis of luminescent graphene quantum dots with high quantum yield and their toxicity study. *Plos One* **10**, e0144906.

Kamangar, F., Chow, W. H., Abnet, C. C., and Dawsey, S. M. (2009). Environmental causes of esophageal cancer. *Gastroenterol. Clin. North Am.* **38**, 27–57. vii.

Kim, J., Nafiujjaman, M., Nurunnabi, M., Lee, Y. K., and Park, H. K. (2016). Hemorheological characteristics of red blood cells exposed to surface functionalized graphene quantum dots. *Food Chem. Toxicol.* **97**, 346–353.

Lee, J. H., and Paull, T. T. (2005). ATM activation by DNA double-strand breaks through the Mre11-Rad50-Nbs1 complex. *Science* **308**, 551–554.

Li, M., Ma, Y., Huang, P., Du, A., Yang, X., Zhang, S., Xing, C., Liu, F., and Cao, J. (2015). Lentiviral DDX46 knockdown inhibits growth and induces apoptosis in human colorectal cancer cells. *Gene* **560**, 237–244.

Li, Y., Hu, Y., Zhao, Y., Shi, G. Q., Deng, L. E., Hou, Y. B., and Qu, L. T. (2011). An Electrochemical avenue to green-luminescent graphene quantum dots as potential electron-acceptors for photovoltaics. *Adv. Mater.* **23**, 776.

Liu, Y. Y., Luo, Y., Wu, J., Wang, Y. S., Yang, X. Y., Yang, R., Wang, B. Q., Yang, J. R., and Zhang, N. (2013). Graphene oxide can induce in vitro and in vivo mutagenesis. *Sci. Rep.* **3**,

Madani, S. Y., Shabani, F., Dwek, M. V., and Seifalian, A. M. (2013). Conjugation of quantum dots on carbon nanotubes for medical diagnosis and treatment. *Int. J. Nanomed.* **8**, 941–950.

Malumbres, M., and Barbacid, M. (2009). Cell cycle, CDKs and cancer: A changing paradigm. *Nat. Rev. Cancer* **9**, 153–166.

Marechal, A., and Zou, L. (2013). DNA Damage sensing by the ATM and ATR kinases. *Cold Spring Harb. Perspect. Biol.* **5**, a012716.

Markovic, Z. M., Ristic, B. Z., Arsikin, K. M., Klisic, D. G., Harhaji-Trajkovic, L. M., Todorovic-Markovic, B. M., Kepic, D. P., Kravic-Stevovic, T. K., Jovanovic, S. P., Milenkovic, M. M., *et al.*, (2012). Graphene quantum dots as autophagy-inducing photodynamic agents. *Biomaterials* **33**, 7084–7092.

McConnell, K. R., Dynan, W. S., and Hardin, J. A. (1997). The DNA-dependent protein kinase catalytic subunit (p460) is cleaved during Fas-mediated apoptosis in Jurkat cells. *J. Immunol.* **158**, 2083–2089.

Michl, J., Zimmer, J., Buffa, F. M., McDermott, U., and Tarsounas, M. (2016). FANCD2 limits replication stress and genome instability in cells lacking BRCA2. *Nat. Struct. Mol. Biol.* **23**, 755.

Moldovan, G. L., and D'Andrea, A. D. (2009). How the fanconi anemia pathway guards the genome. *Annu. Rev. Genet.* **43**, 223–249.

Pagliarini, V., Giglio, P., Bernardoni, P., De Zio, D., Fimia, G. M., Piacentini, M., and Corazzari, M. (2015). Downregulation of E2F1 during ER stress is required to induce apoptosis. *J. Cell Sci.* **128**, 1166–1179.

Pasquier, E., and Kavallaris, M. (2008). Microtubules: A dynamic target in cancer therapy. *Iubmb Life* **60**, 165–170.

Poruchynsky, M. S., Komlodi-Pasztor, E., Trostel, S., Wilkerson, J., Regairaz, M., Pommier, Y., Zhang, X., Kumar Maity, T., Robey, R., Burotto, M., *et al.*, (2015). Microtubule-targeting agents augment the toxicity of DNA-damaging agents by disrupting intracellular trafficking of DNA repair proteins. *Proc. Natl. Acad. Sci. U.S.A.* **112**, 1571–1576.

Qin, Y. R., Zhou, Z. W., Pan, S. T., He, Z. X., Zhang, X. J., Qiu, J. X., Duan, W., Yang, T. X., and Zhou, S. F. (2015). Graphene quantum dots induce apoptosis, autophagy, and inflammatory response via p38 mitogen-activated protein kinase and nuclear factor-kappa B mediated signaling pathways in activated THP-1 macrophages. *Toxicology* **327**, 62–76.

Qiu, J. C., Li, D. S., Mou, X. N., Li, J. H., Guo, W. B., Wang, S., Yu, X., Ma, B. J., Zhang, S., Tang, W., *et al.* (2016). Effects of graphene quantum dots on the self-renewal and differentiation of mesenchymal stem cells. *Adv. Healthcare Mater.* **5**, 702–710.

Ratnikova, T. A., Govindan, P. N., Salonen, E., and Ke, P. C. (2011). In vitro polymerization of microtubules with a fullerene derivative. *Acs Nano* **5**, 6306–6314.

Schwab, R. A., Nieminuszczy, J., Shah, F., Langton, J., Martinez, D. L., Liang, C. C., Cohn, M. A., Gibbons, R. J., Deans, A. J., and Niedzwiedz, W. (2015). The fanconi anemia pathway maintains genome stability by coordinating replication and transcription. *Mol. Cell* **60**, 351–361.

Shamanna, R. A., Lu, H., Croteau, D. L., Arora, A., Agarwal, D., Ball, G., Aleskandarany, M. A., Ellis, I. O., Pommier, Y., Madhusudan, S., *et al.*, (2016). Camptothecin targets WRN protein: Mechanism and relevance in clinical breast cancer. *Oncotarget* **7**, 13269–13284.

Shang, Z., Yu, L., Lin, Y. F., Matsunaga, S., Shen, C. Y., and Chen, B. P. (2014). DNA-PKcs activates the Chk2-Brca1 pathway during mitosis to ensure chromosomal stability. *Oncogenesis* **3**, e85.

Shen, J., Zhu, Y., Yang, X., and Li, C. (2012). Graphene quantum dots: Emergent nanolights for bioimaging, sensors, catalysis and photovoltaic devices. *Chem. Commun. (Camb.)* **48**, 3686–3699.

Tian, X., Xiao, B. B., Wu, A. Q., Yu, L., Zhou, J. D., Wang, Y., Wang, N., Guan, H., and Shang, Z. F. (2016). Hydroxylated-graphene quantum dots induce cells senescence in both p53-dependent and -independent manner. *Toxicol. Res.* **5**, 1639–1648.

Tian, X., Yang, Z. X., Duan, G. X., Wu, A. Q., Gu, Z. L., Zhang, L. L., Chen, C. Y., Chai, Z. F., Ge, C. C., and Zhou, R. H. (2017). Graphene oxide nanosheets retard cellular migration via disruption of actin cytoskeleton. *Small* **13**, 1602133.

Vinogradov, S., and Wei, X. (2012). Cancer stem cells and drug resistance: The potential of nanomedicine. *Nanomedicine* **7**, 597–615.

Wang, C., Wu, C., Zhou, X., Han, T., Xin, X., Wu, J., Zhang, J., and Guo, S. (2013). Enhancing cell nucleus accumulation and DNA cleavage activity of anti-cancer drug via graphene quantum dots. *Sci. Rep.* **3**, 2852.

Wang, D., Zhu, L., Chen, J. F., and Dai, L. M. (2015). Can graphene quantum dots cause DNA damage in cells? *Nanoscale* **7**, 9894–9901.

Wang, S. J., Cole, I. S., and Li, Q. (2016). The toxicity of graphene quantum dots. *RSC Adv.* **6**, 89867–89878.

Wang, T. T., Zhu, S. J., and Jiang, X. E. (2015). Toxicity mechanism of graphene oxide and nitrogen-doped graphene quantum dots in RBCs revealed by surface-enhanced infrared absorption spectroscopy. *Toxicol. Res.* **4**, 885–894.

Wang, X., Sun, X., Lao, J., He, H., Cheng, T., Wang, M., Wang, S., and Huang, F. (2014). Multifunctional graphene quantum dots for simultaneous targeted cellular imaging and drug delivery. *Colloid. Surf. B Biointerfaces* **122**, 638–644.

Wang, Y., Deng, O., Feng, Z., Du, Z., Xiong, X., Lai, J., Yang, X., Xu, M., Wang, H., Taylor, D., *et al.* (2016). RNF126 promotes homologous recombination via regulation of E2F1-mediated BRCA1 expression. *Oncogene* **35**, 1363–1372.

Wang, Z., Xia, J., Zhou, C., Via, B., Xia, Y., Zhang, F., Li, Y., Xia, L., and Tang, J. (2013). Synthesis of strongly green-photoluminescent graphene quantum dots for drug carrier. *Colloid. Surf. B Biointerfaces* **112**, 192–196.

Wang, Z. G., Zhou, R., Jiang, D., Song, J. E., Xu, Q., Si, J., Chen, Y. P., Zhou, X., Gan, L., Li, J. Z., *et al.* (2015). Toxicity of graphene quantum dots in zebrafish embryo. *Biomed. Environ. Sci.* **28**, 341–351.

Wu, C. Y., Wang, C., Han, T., Zhou, X. J., Guo, S. W., and Zhang, J. Y. (2013). Insight into the cellular internalization and cytotoxicity of graphene quantum dots. *Adv. Healthcare Mater.* **2**, 1613–1619.

Yan, Y. Q., Xu, Q. Z., Wang, L., Sui, J. L., Bai, B., and Zhou, P. K. (2006). Vanillin derivative 6-bromine-5-hydroxy-4-methoxybenzaldehyde-elicited apoptosis and G2/M arrest of Jurkat cells proceeds concurrently with DNA-PKcs cleavage and Akt inactivation. *Int. J. Oncol.* **29**, 1167–1172.

Yuan, X. C., Liu, Z. M., Guo, Z. Y., Ji, Y. H., Jin, M., and Wang, X. P. (2014). Cellular distribution and cytotoxicity of graphene quantum dots with different functional groups. *Nanoscale Res. Lett.* **9**, 108.

Zhao, Y. L., Liu, Q., Shakoor, S., Gong, J. R., and Wang, D. Y. (2015). Transgenerational safety of nitrogen-doped graphene quantum dots and the underlying cellular mechanism in Caenorhabditis elegans. *Toxicol. Res.* **4**, 270–280.

Zheng, X. T., Than, A., Ananthanaraya, A., Kim, D. H., and Chen, P. (2013). Graphene quantum dots as universal fluorophores and their use in revealing regulated trafficking of insulin receptors in adipocytes. *ACS Nano* **7**, 6278–6286.

Zhou, X. J., Zhang, Y., Wang, C., Wu, X. C., Yang, Y. Q., Zheng, B., Wu, H. X., Guo, S. W., and Zhang, J. Y. (2012). Photo-fenton reaction of graphene oxide: A new strategy to prepare graphene quantum dots for DNA cleavage. *ACS Nano* **6**, 6592–6599.

Zhu, H., Guo, F. J., Zhao, W., Zhou, J., Liu, Y., Song, F., and Wang, Y. (2012). ATF4 and IRE1alpha inhibit DNA repair protein DNA-dependent protein kinase 1 induced by heat shock. *Mol. Cell. Biochem.* **371**, 225–232.

Zhu, S. J., Zhang, J. H., Qiao, C. Y., Tang, S. J., Li, Y. F., Yuan, W. J., Li, B., Tian, L., Liu, F., Hu, R., *et al.*, (2011). Strongly green-photoluminescent graphene quantum dots for bioimaging applications. *Chem. Commun.* **47**, 6858–6860.